# Superheating and melting-point depression of Pb nanoparticles embedded in Al matrices

By H. W. SHENG†, G. REN‡, L. M. PENG‡, Z. Q. HU†, and K. LU†§

†National Key Laboratory for RSA, Institute of Metal Research, Chinese
Academy of Sciences, Shenyang 110015, PR China
‡Beijing Laboratory of Electron Microscopy, Chinese Academy of Sciences,
Beijing 100080, PR China
§International Center for Materials Physics, Institute of Metal Research, Chinese
Academy of Sciences, Shenyang 110015, PR China

## ABSTRACT

Two kinds of Pb–Al granular sample (with nanometre-sized Pb particles embedded in an Al matrix) were prepared by using melt-spinning and ball-milling techniques. The Pb particles were synthesized with similar particle sizes, about 5–30 nm in diameter, but were observed to have different Pb–Al interfaces for samples prepared using different approaches. In the melt-spun Pb–Al samples, the Pb nanoparticles were seen to have an epitaxial relationship with the Al matrix, while the Pb particles in the ball-milled sample were seen to be randomly oriented with respect to the Al matrix. The melting behaviour of the Pb particles was investigated by differential scanning calorimetry. It was found that the faceted Pb nanoparticles in the melt-spun sample could be superheated by about 11–40 K, whereas the irregularly shaped Pb particles in the ball-milled sample melted about 13 K below its equilibrium point. We suggest that different interface structures, which cause variations in energy differences between solid-Pb–solid-Al and liquid-Pb–solid-Al interfaces, are responsible for the different melting behaviour of Pb nanoparticles.

Although melting is ubiquitous in nature, the melting mechanism is still an open question to scientists. Since Tagaki (1954) discovered the melting-point depression of metallic thin films, many cases have been reported where metallic particles or thin films melt below their equilibrium melting points (Wronski 1967, Buffat and Borel 1976, Boyer 1985, Allen, Bayle, Gile and Jesser 1986). Some other observations showed, however, that the embedded particles may also be superheated above their equilibrium melting temperatures (Allen, Gile and Jesser 1980, Rossouw and Donnelly 1985, Däges, Gleiter and Perepezko 1986, Saka, Nishikawa and Imura 1988, Zhang and Cantor 1991). Many pieces of evidence suggest that the surface (or interface) plays an important role in melting processes (Couchman and Jesser 1977a,b, Cahn 1986). Recent experiments revealed that melting is a surface-initiated process in some systems with a depressed melting point. The thickness of a surface-melted liquid film, which coats the solid core at a temperature lower than the bulk melting temperature $T_m$, is found to be proportional to $T_0/(T_m - T)$, where $T_0$ is a constant. When the temperature approaches the bulk melting point, the thickness of the liquid–solid films diverges (Frenken and van der Veen 1985, Pluis, Denier van der Gon, Frenken and van der Veen 1987, Lereah, Deutscher, Cheyssac and Kofman 1989, 1990, Ben David *et al.* 1995).

However, this scenario of melting is questionable because of the superheating of the entrained particles, which has been related to strain-energy effects (Allen *et al.* 1980, Malhotra and Van Aken 1995), interface-energy effects (Saka *et al.* 1988) and kinetic barriers to nucleation (Spiller 1982, Däges, Gleiter and Perepezko 1986, Zhang and Cantor 1991). It is worth noting that the superheated particles often have an epitaxial relationship with the containing hosts. Cahn (1986) suggested that the observed superheating originates from the epitaxy between the embedded particles and the matrix, and no substantial superheating is expected for the incoherent interfaces. Therefore, it is of significance to carry out a comparative study of the melting behaviour of embedded particles with different types of interface in order to clarify the intrinsic effect of the interface structures on melting processes.

In the present work, we chose Pb nanoparticles embedded in Al matrices as model samples. Two types of Pb–Al interface structures in the granular specimens with nanometre-sized Pb particles were constructed: firstly semicoherent Pb–Al interfaces in a melt-spun sample, and secondly incoherent interfaces in a ball-milled specimen. A comparative investigation of their melting behaviour was performed, and both superheating and the melting-point depression phenomena were observed experimentally.

An alloy ingot with a composition of Al–10 wt% Pb was prepared by arc melting of 99·999% pure Al and Pb in water-cooled copper crucibles under an Ar atmosphere. Thin ribbons of Pb–Al, 2–3 mm wide, 20 $\mu$m thick and a few metres long, were obtained by means of the melt-spinning technique. The overall composition of the as-quenched ribbon remained Al–10 wt% Pb. Commercial elemental powder blends of Al and Pb (purity, 99·999%; particles, less than 100 mesh) with the same composition of the melt-spun sample were used as starting materials for the ball-milled samples. Ball milling was performed in a vibratory ball mill. High-hardness, chrome steel balls of good wear resistance were used; the ball-to-powder weight ratio was 30 to 1. The as-quenched and as-milled Al–Pb samples were examined using X-ray diffraction (XRD), energy-dispersive X-ray spectroscopy (EDXS), transmission electron microscopy (TEM) and high-resolution transmission electron microscopy (HRTEM) techniques. XRD experiments were carried out on a Rigaku X-ray diffractometer (D/max-ra; 12 kW) with Cu K$^\alpha$ radiation. TEM and HRTEM were conducted on a JEOL-2010 microscope. Specimens for TEM and HRTEM observations were prepared by ion thinning for the melt-spun ribbons and for the as-milled samples (which were consolidated from the as-milled powders).

The melting behaviour of Pb was monitored using a Perkin–Elmer differential scanning calorimeter (DSC-7), with a sensitivity of 0·04 mJ s$^{-1}$ for energy measurements. Either the melt-spun ribbons or the as-milled samples (compacted) were sealed in Al pans and heated in a flowing Ar atmosphere at a constant heating rate of 10°C min$^{-1}$. The temperature for differential scanning calormetry (DSC) measurements was calibrated by pure In and Zn standard samples with an accuracy of ±0·02 K.

Al–Pb is a typical immiscible binary system (Massalski 1986). Despite the non-equilibrium processing of the Al–10 wt% Pb alloy (e.g. rapid quenching and ball milling), we did not detect any solubility between Al and Pb from XRD experiments. Figure 1(*a*) shows a bright-field TEM image of the Pb–Al melt-spun ribbon. It can be seen that the faceted Pb particles are uniformly distributed throughout the Al matrix. The Pb particle sizes are in the range 5–30 nm with a mean diameter of 11 nm, as shown in fig. 1(*b*). In addition, moiré fringes in the images of the small

Fig. 1



(a)

(c)          (d)

(b)

(e)

(f)
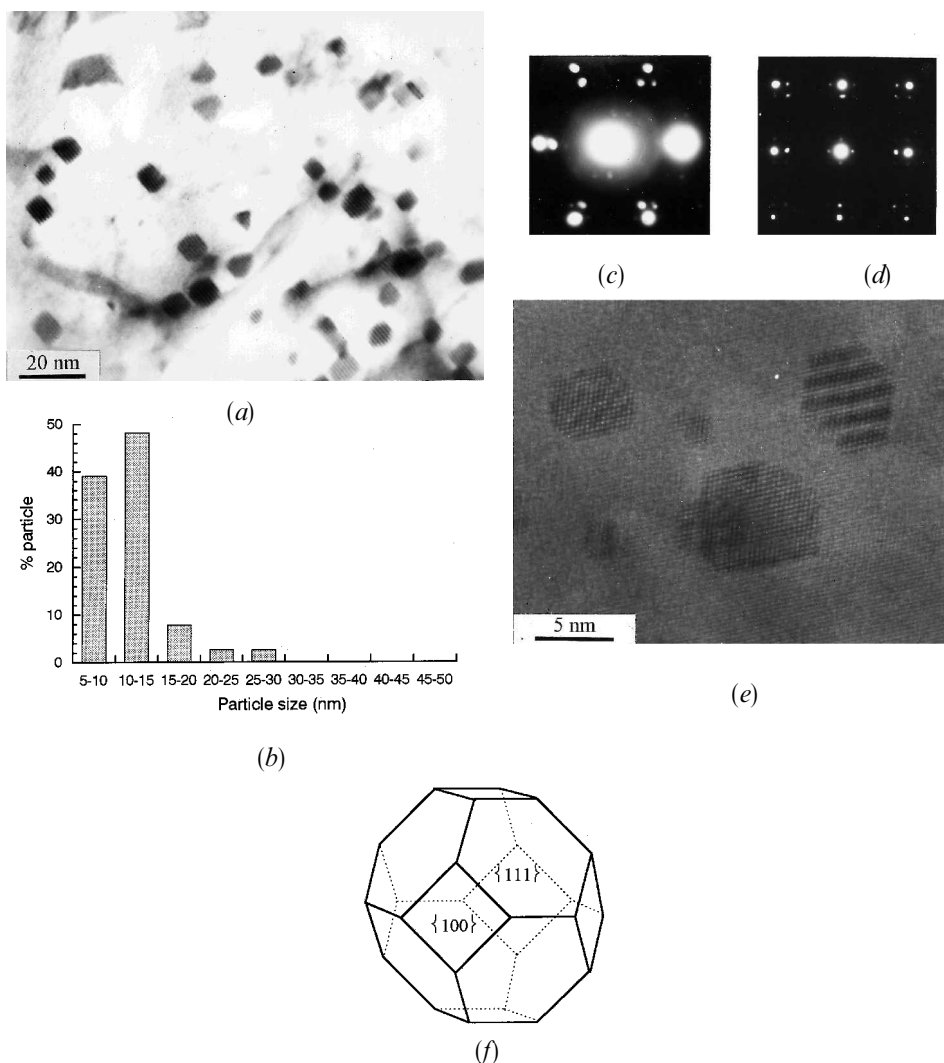
(a) A typical bright-field transmission electron micrograph of melt-spun Al–10 wt% Pb; (b) a histogram showing the distribution of the Pb particles; (c), (d) SAED patterns from melt spun Al–10 wt% Pb, with the beam direction parallel to the (c) $\langle 110 \rangle_{Al}$ and (d) $\langle 111 \rangle_{Al}$ zone axes, showing a cube–cube orientational relationship between the Pb particles and the Al matrix; (e) HRTEM image corresponding to (c), showing the hexagonal-shaped Pb particles and the semicoherent Pb–Al interface; (f) schematic diagram of the truncated octahedral Pb particle shape.

Pb particle are clearly seen, indicating that the Pb–Al interface is highly ordered. Figures 1(c) and (d) show typical electron diffraction patterns from Al $\langle 110 \rangle$ and $\langle 111 \rangle$ zones for the melt-spun Pb–Al sample. These results agree with those reported previously (Moore, Chattopadhyay and Cantor 1987, Zhang and Cantor 1991), that is the Pb particles in the melt-spun Al–10 wt% Pb exhibited a cube–cube orientational relationship with the surrounding Al matrix ($\{111\}_{Al}\|\{111\}_{Pb}$ and

$\langle 110 \rangle_{Al} \| \langle 110 \rangle_{Pb}$). Figure 1(*e*) shows a HRTEM image corresponding to fig. 1(*c*). In addition to the semicoherent Pb–Al interface, the Pb particles exhibited hexagonal shapes perpendicular to the Al $\langle 110 \rangle$ zone axis, indicating that the particle shapes were truncated octahedra bounded by {111} and {100} facets, as schematically shown in fig. 1(*f*).

In the ball-milling experiments, we found that the Pb particle size decreased with milling time and tended to the nanometre regime. The final product was a nano-structured mixture of pure Al and Pb phases. No alloying effect was observed between Al and Pb even when the grains were extremely small. The details of the structural changes during ball milling will be reported elsewhere (Sheng *et al.* 1995).

In order to remove the microstrain and to ensure the grain growth of Al in the Pb–Al sample, the Pb–Al powder mixture milled for 10 h was annealed at 330°C for 10 min. A typical TEM image of the annealed Pb–Al sample is shown in fig. 2(*a*). It is evident that the Pb particles, which are in the form of irregular shapes, are embedded in the Al matrix. The Pb nanoparticles, about 5–50 nm in diameter, are uniformly distributed in the Al matrix, with a statistical mean diameter of 15 nm, which is in satisfactory agreement with the XRD measurements. Figure 2(*c*) is a selected-area

Fig. 2
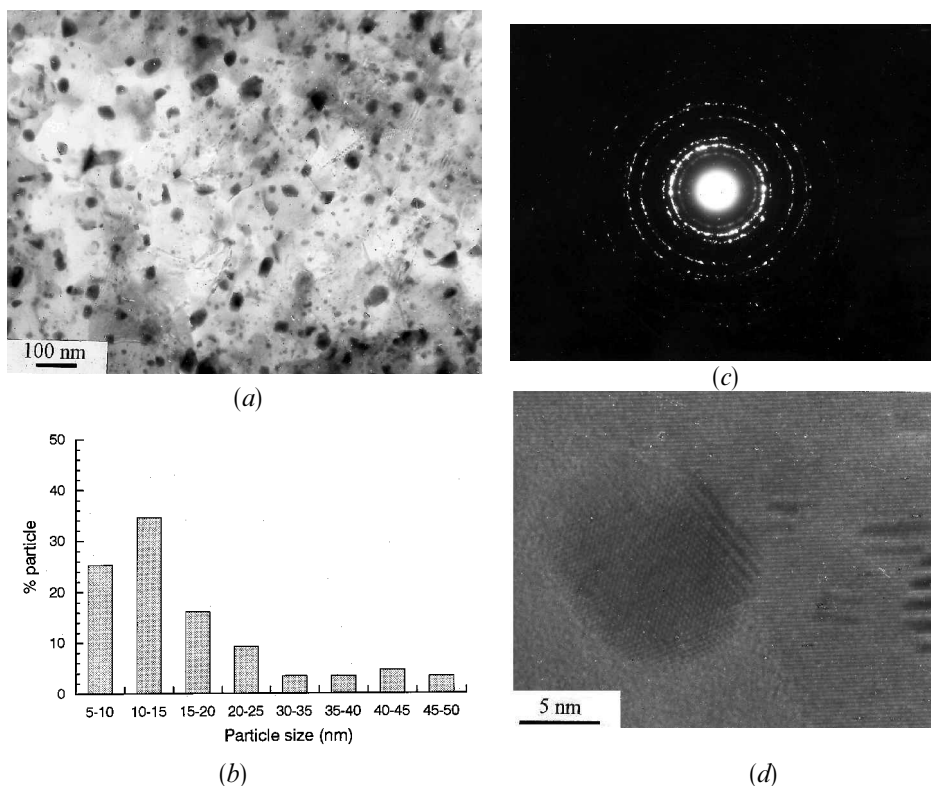


(*a*) A bright-field TEM image of ball milled Al–10 wt% Pb; (*b*) a histogram showing the distribution of the Pb particles; (*c*) SAED pattern corresponding to (*a*); (*d*) HRTEM image showing the morphology of the Pb particles and the incoherent Pb–Al interface.

electron diffraction pattern for the as-annealed Pb–Al sample, from which both the Pb and the Al phases are found to be in random orientations. No epitaxial orientational relationship between Pb and Al can be identified. HRTEM observations of Pb–Al milled powder have been performed in order to explore the morphologies of embedded Pb particles, and a typical HRTEM image is shown in fig. 2(d). Nanometre-sized Pb particles are clearly found located either inside Al grains or at the Al grain boundaries. Interlayer phases between Pb–Al have not been found in our HRTEM observations. Evidently, morphologies and the Pb–Al interface structures in the as-milled sample are different from those in the melt-spun sample.

Figures 3(a) and (b) show typical DSC endotherms for the melting of Pb nanoparticles in the melt-spun and ball-miled Al–10 wt% Pb specimens, respectively. For the melt-spun Pb–Al specimen (fig. 3(a)), the Pb particles melted with a sharp endotherm at an onset temperature of $322 \cdot 4°C$, followed by a broad endothermic peak over a temperature range 338–367°C. After the sample was heated to 400°C

Fig. 3



(a)



(b)
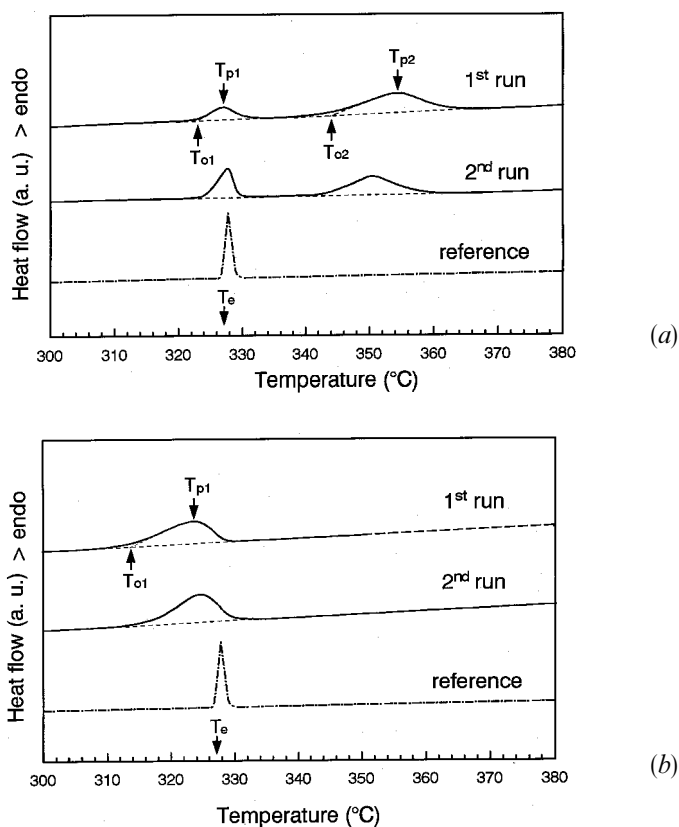
DSC traces of melting endotherms for the Pb particles in (a) the melt-spun Al–10 wt% Pb sample and (b) the ball-milled Al–10 wt% Pb sample, at a heating rate of $10°C \, min^{-1}$ (a.u., arbitrary units). Characteristic temperatures for melting (onset temperature $T_o$ and peak temperature $T_p$) are illustrated in the DSC curve. The reference curve is the melting DSC curve for the 'bulk' Pb in the as-cast Pb–Al alloy. $T_e$ is the equilibrium melting temperature of pure Pb.

and cooled to 300°C, a second DSC run of the same sample was performed. No substantial change in the DSC curve was found. The results are similar to those reported by Zhang and Cantor (1991). For comparison, fig. 3 also gives the reference curves of melting of the 'bulk' Pb (micrometre-sized) in the as-cast Pb–Al sample. The first endothermic peak, which coincides with that of the reference melting peak, may be attributed to the melting of relatively large Pb particles which have not been reduced in size during melt spinning. The second broad endothermic peak, on the other hand, might be reasonably explained by the melting of faceted Pb nanoparticles in the Al maxtrix. The *in situ* heating TEM experiments confirmed that the ultrafine Pb particles (5–30 nm) in the as-quenched Pb–Al sample melt at temperatures far above the equilibrium melting point of Pb (by about 11–40 K) (Sheng *et al.* 1995), which agrees well with the second endothermic peak in the DSC curve. In fact, similar phenomena have been observed by Zhang and Cantor (1991), namely that the Pb nanoparticles in the melt-spun Pb–Al sample can be superheated by 0–40 K. The characteristic temperatures of the melting peaks appearing on the DSC curves are summarized in the table.

Figure 3(*b*) shows the DSC curves of the annealed Pb–Al powders milled for 10 h. A flat endothermic peak corresponding to the melting of Pb particles appears in the DSC curve. The endotherm peak spans a wide temperature range, with an onset temperature of 314°C. Compared with the melting peak of the reference 'bulk' Pb sample, it is easily discerned that the melting temperature of the irregular nanometre-sized Pb particles in the Al matrix is depressed. A second run of the same sample after cooling from 350°C does not show any change in the shape of the endothermic peak, indicating that no substantial particle coarsening takes place up to 350°C. The melting-point depression of the Pb particles in the Al matrix is well reproducible. The characteristic temperatures for the melting endothermic peak are listed in the table.

Owing to the different synthesis processes, many factors may affect the melting behaviour of Pb nanoparticles in the Al matrices, such as introduced impurities and microstrains during milling and quenching processes. In the ball-milled samples, we detected traces of iron impurities from contamination (about $0.003 \, \text{wt\%} \, \text{h}^{-1}$). However, such a small amount of Fe impurities can hardly affect the melting beha-

The onset and peak temperatures of melting of Pb in Al–Pb samples under different conditions. The change in the melting point with respect to the onset of the melting of the 'bulk' Pb in as-cast Al–Pb, $\Delta T = T_0 - T_m$, is also shown.

| Sample | Peak 1 | | | Peak 2 | | |
|---|---|---|---|---|---|---|
| | $T_{o1}(°C)$ | $T_{p1}(°C)$ | $\Delta T(°C)$ | $T_{o2}(°C)$ | $T_{p2}(°C)$ | $\Delta T(°C)$ |
| Melt spun (5–30 nm), first | 323·4 | 327·2 | −3·8 | 344·1 | 354·2 | +21·9 |
| Melt spun (5–30 nm), second | 324·8 | 328·0 | −2·4 | 342·2 | 350·0 | +20 |
| Ball milled (5–50 nm), first | 314·0 | 321·6 | −13·2 | — | — | — |
| Ball milled (5–50 nm), second | 316·2 | 322·0 | −11 | — | — | — |
| As cast reference | 327·2 | 327·9 | 0 | — | — | — |

viour of the Pb particles. Our results show that in the melt-spun Pb–Al ribbon with an addition of iron (2 wt%), the embedded Pb particles are also superheated by about 20–40 K as determined by DSC. The energy stored by cold work may serve as another reason for the lowering of the melting temperature of Pb particles (Bahk and Ashby 1975) but here, in our as-milled samples, the subsequent remelting runs did not remove the melting-point depression of Pb particles, implying that the energy stored by ball milling is not a dominant factor for the melting-point depression. In conclusion, the external factors from the synthesis methods cannot account for the change in the melting behaviour of Pb particles in the Pb–Al dispersions.

The intrinsic mechanism for superheating is still controversial. More recently, Malhotra and Van Aken (1995) argued that the volume transformation stress upon melting was the major factor for the melting temperature elevation in microparticles. However, this does not seem to be the case in the melt-spun samples. This is because in the ball-milled Pb–Al particles, although there exist substantial amounts of Pb particles embedded in the Al grain interior, melting-point depression rather than superheating was observed.

We note that in the two kinds of Pb–Al dispersion, the Pb–Al interface structures are different. An alternative interpretation of the melting-point change of the Pb particles may be related to the interface effects as follows.

From a thermodynamic point of view, the size-dependent melting point for the embedded Pb particles can be described by the Couchman–Jesser (1977a,b) equation

$$\frac{T_m}{T_0} = 1 - \frac{3(\sigma_{sm} - \sigma_{lm})/\rho r - \Delta E}{\Delta H_m^e},$$

where $\rho = (\rho_s + \rho_l)/2$, $T_m$ is the melting point of the Pb particles, $T_0$ is the equilibrium melting temperature of the bulk Pb, $\sigma_{sm}$ and $\sigma_{lm}$ are the interface energies of the solid-Pb–solid-Al and liquid-Pb–solid-Al interfaces, $\Delta E$ is the difference between the energy densities of solid and liquid Pb particles, $\Delta H_m^e$ is the fusion enthalpy of bulk Pb in the equilibrium state and $r$ is the mean radius of Pb particles. It can be seen that, neglecting $\Delta E$, the melting point of Pb can be either increased or decreased, depending on the sign of $\sigma_{sm} - \sigma_{lm}$, which is closely related to the nature of the Pb–Al interface configurations.

In the ball-milled Pb–Al samples the randomly oriented Pb crystallites are incoherent with the Al matrix, and both interface enthalpy and interface entropy are assumed to be higher than those of the coherent or semicoherent interface. On the assumption that the liquid Pb–solid Al interfaces in both dispersions are the same, the interface energy difference $\sigma_{sm} - \sigma_{lm}$ for the as-milled Pb–Al sample will be larger than those for the as-quenched Pb–Al ribbon. Thus, according to the Couchman–Jesser equation, the variation in the interfacial energy difference, that is $\sigma_{sm} - \sigma_{lm}$ will lead to a different melting behaviour for the embedded Pb particles. It can be inferred that, in the as-milled Pb–Al samples (with incoherent Pb–Al interfaces), $\sigma_{sm}$ is larger than $\sigma_{lm}$ while, in the as-quenched Pb–Al samples (with an epitaxial relationship between Pb and the Al matrix) $\sigma_{sm}$ is smaller than $\sigma_{lm}$.

From a kinetics point of view, in the ball-milled Pb–Al sample, owing to the roughness and disordered regions in the Pb–Al interface, there might be more nucleation sites for melting than in the as-quenched samples, and melting-point depression is therefore kinetically feasible. On the other hand, the faceted Pb particles formed in the melt-spun samples may have more difficulty in nucleating on melting on the ordered facets for lack of favourable nucleation sites such as pores

or dislocations, thus existing to higher temperatures as suggested by Zhang and Cantor (1991).

In summary, we prepared two kinds of nanometre-sized Pb particles embedded in Al matrices by using melt-spinning and ball-milling techniques. In the melt-spun samples, faceted Pb particles are typically 5–30 nm in diameter and have an epitaxial relationship with the Al matrix, while in the ball-milled Pb–Al sample the Pb particles are randomly oriented with respect to the Al matrix. The melting behaviours of the two kinds of Pb particle are fundamentally different. In the melt-spun ribbon, the faceted Pb particles can be superheated by about 11–40 K, but in the ball-milled Pb–Al samples, in which grain sizes were similar to those in the melt-spun samples, the Pb particles melted about 13 K below the equilibrium melting temperature. It is concluded that different interface structures are responsible for the different melting behaviours of Pb particles embedded in the Al matrix. In other words, the melting processes of Pb nanoparticles are dominantly controlled by the nature of the Pb–Al interface structures.

REFERENCES

ALLEN, G. L., BAYLE, R. A., GILE, W. W., and JESSER, W. A., 1986, *Thin Solid Films*, **144**, 297.
ALLEN, G. L., GILE, W. W., and JESSER, W. A., 1980, *Acta metall.*, **28**, 1965.
BAHK, S., and ASHBY, M. F., 1975, *Script metall.*, **9**, 129.
BEN DAVID, T., LEREAH, Y., DEUTSCHER, G., KOFMAN, R., and CHEYSSAC, P., 1995, *Phil. Mag.* A, **71**, 1135.
BOYER, L. L., 1985, *Phase Transitions*, **5**, 1.
BUFFAT, P. H., and BOREL, J. P., 1976, *Phys. Rev.* A, **13**, 2287.
COUCHMAN, P. R., and JESSER, W. A., 1977a, *Phil. Mag.*, **35**, 787; 1977b, *Nature*, **269**, 481.
CAHN, R. W., 1986, *Nature*, **323**, 668.
DÄGES, J., GLEITER, H., and PEREPEZKO, J. H., 1986, *Phys. Lett.*, **119**, 79.
FRENKEN, J. H. and VAN DEN VEEN, J. F., 1985, *Phys. Rev. Lett.*, **54**, 134.
LEREAH, Y., DEUTSCHER, G., CHEYSSAC, P., and KOFMAN, R., 1989, *Europhys. Lett.*, **8**, 53; 1990, *Ibid.*, **12**, 709.
MALHOTRA, A. K., and VAN AKEN, D. C., 1995, *Phil Mag.* A, **71**, 949.
MASSALSKI, T. B., 1986, *Binary Alloy Phase Diagrams* (Metals Park, Ohio: American Society for Metals).
MOORE, K. I., CHATTOPADHYAY, K., and CANTOR, B., 1987, *Proc. R. Soc.* A, **414**, 499.
PLUIS, B., DENIER VAN DEN GON, A. W., FRENKEN, J. W. M., and VAN DER VEEN, J. F., 1987, *Phys. Rev. Lett.*, **59**, 2687.
ROSSOUW, C. J., and DONNELLY, S. F., 1985, *Phys. Rev. Lett.*, **55**, 2960.
SAKA, H., NISHIKAWA, Y., and IMURA, T., 1988, *Phil. Mag.* A, **57**, 895.
SHENG, H. W. *et al.*, 1995 (to be published).
SPILLER, D. G. T., 1982, *Phil. Mag.* A, **46**, 535.
TAKAGI, M., 1954, *J. phys. Soc. Japan*, **9**, 359.
WRONSKI, C. R. M., 1967, *Br. J. appl. Phys.*, **18**, 1731.
ZHANG, D. L., and CANTOR, B., 1991, *Acta metall. mater.*, **39**, 1595.